

Higgs masses and Electroweak Precision Observables in the Lepton-Flavor-Violating MSSM

M.E. GÓMEZ^{1*}, T. HAHN^{2†}, S. HEINEMEYER^{3‡}, AND M. REHMAN^{3§¶}

¹*Department of Applied Physics, University of Huelva, 21071 Huelva, Spain*

²*Max-Planck-Institut für Physik, Föhringer Ring 6,
D-80805 München, Germany*

³*Instituto de Física de Cantabria (CSIC-UC), Santander, Spain*

Abstract

We study the effects of Lepton Flavor Violation (LFV) in the scalar lepton sector of the MSSM on precision observables such as the W -boson mass and the effective weak leptonic mixing angle, and on the Higgs-boson mass predictions. The slepton mass matrices are parameterized in a model-independent way by a complete set of dimensionless parameters which we constrain through LFV decay processes and the precision observables. We find regions where both conditions are similarly constraining. The necessary prerequisites for the calculation have been added to FeynArts and FormCalc and are thus publicly available for further studies. The obtained results are available in FeynHiggs.

*email: mario.gomez@dfa.uhu.es

†email: hahn@feynarts.de

‡email: Sven.Heinemeyer@cern.ch

§email: rehman@ifca.unican.es

¶MultiDark Scholar

1 Introduction

Lepton Flavor Violating (LFV) processes provide one of the most interesting probes to physics beyond the Standard Model (SM) of particle physics. All SM interactions preserve lepton flavor number and therefore a measurement of any (charged) LFV process would be an unambiguous signal of physics beyond the SM and provide interesting information on the involved flavor mixing, as well as on the underlying origin for this mixing (for a review see Ref. [1], for instance).

The data from past and ongoing neutrino oscillation experiments, as well as from cosmology and astrophysics, have confirmed that neutrinos have different non-zero masses and that the three neutrino flavors ν_e, ν_μ, ν_τ mix to form three mass eigenstates. This implies non-conservation of lepton flavor, clearly beyond the SM. Thus, lepton-flavor-violating processes are expected in the lepton sector just as quark-flavor-violating processes arise in the quark sector.

Within the Minimal Supersymmetric Standard Model (MSSM) [2], LFV can occur in the scalar lepton sector. The most general way to introduce slepton flavor mixing within the MSSM is through the off-diagonal soft-SUSY-breaking parameters (both mass parameters and trilinear couplings) in the slepton sector. The off-diagonality in the slepton mass matrix reflects the misalignment (in flavor space) between lepton and slepton mass matrices, which cannot be diagonalized simultaneously. This misalignment can have various origins; for instance, off-diagonal slepton mass matrix entries can be generated by Renormalization Group Equations running from high energies, where heavy right-handed neutrinos are assumed to be active, down to low energies where LFV processes can occur [3, 4].

In this work we do not investigate the possible dynamical origin of this lepton–slepton misalignment, nor particular predictions for off-diagonal slepton soft-SUSY-breaking mass terms in specific SUSY models, but instead parameterize the slepton mass matrix and explore the phenomenological implications of LFV on various observables.

Specifically, we write the off-diagonal slepton mass matrix elements in terms of a complete set of generic dimensionless parameters $\delta_{\{12,13,23\}}^{\{LL,LR,RL,RR\}}$, where L, R refers to the left-/right-handed SUSY partner of the corresponding leptonic degree of freedom and 1, 2, 3 are the involved generation indices, and explore the sensitivity of several precision observables to the δ_{ij}^{AB} 's, extending a program carried out for flavor violation in the scalar quark sector [5].

Besides direct searches, which have not turned up evidence for any additional particles so far, SUSY can also be probed through its effects on precision observables via virtual particles, see Ref. [6] for a review. Electroweak precision observables (EWPO) like the W -boson mass or the effective weak leptonic mixing angle have been measured to a very high precision, and the anticipated improved precision in current and future experiments for these observables makes them very sensitive to physics beyond the SM.

Besides EWPO we also explore the effects of LFV on the MSSM Higgs sector, again extending existing analyses on flavor violation in the scalar quark sector [5, 7]. The MSSM Higgs sector consist of two Higgs doublets and predicts five physical Higgs bosons, the light and heavy \mathcal{CP} -even h and H , the \mathcal{CP} -odd A , and the charged Higgs boson H^\pm . At tree level the Higgs sector is described with the help of two parameters: the mass of the A boson, M_A , and $\tan\beta := v_2/v_1$, the ratio of the two vacuum expectation values. After the spectacular discovery of a Higgs particle at the LHC, the precision of the measured mass

value is already below the GeV level [8, 9], and at a future ILC, a precision even below ~ 50 MeV is anticipated [10]. We evaluate the effects of LFV on the predictions of the masses of the light and heavy \mathcal{CP} -even Higgs bosons, M_h and M_H , as well as on the charged Higgs-boson mass M_{H^\pm} . Based on the evaluations in the scalar quark sector [5], theoretical uncertainties from LFV effects on the evaluation of the Higgs-boson masses are substantially larger than the future experimental accuracy could be expected, motivating the analytical calculation of these corrections.

For our calculations we prepared (and thoroughly tested) an add-on model file for FeynArts [11, 12] which adds LFV effects to the existing MSSM model file. No renormalization as in Ref. [13] is included yet (and also not necessary for the present work since the SM is lepton-flavor conserving and hence there is no tree-level contribution). The FormCalc [14] driver files were also modified accordingly. We checked that the LFV Feynman rules yield finite results for all our calculations. The results derived with this setup, the Higgs-boson masses as well as the EWPO, were added to FeynHiggs 2.10.2.

This paper is organized as follows: First we review the main features of the MSSM with general slepton flavor mixing and set the relevant notation for the δ_{ij}^{AB} 's in Sect. 2. The selection of specific MSSM scenarios as well as their experimental restrictions from LFV processes is presented in Sect. 3. The numerical analysis is given in Sect. 4, showing for the first time the LFV effects on the MSSM Higgs boson masses and on the EWPO. Sect. 5 summarizes our conclusions.

2 Calculational Basis

We work in MSSM scenarios with general flavor mixing in the sleptons. Within these MSSM-FV scenarios, lepton flavor violation is induced by the PMNS matrix of the neutrino sector and transmitted by the small neutrino Yukawa couplings which we ignore here. Flavor mixing in the slepton mass matrix is the main generator of LFV. In the following we give a brief overview about the relevant sectors of the MSSM with LFV.

2.1 Scalar lepton sector with LFV

For the slepton sector of the MSSM including LFV contributions we use the same notation as Ref. [20]. The most general hypothesis for flavor mixing in the slepton sector assumes a non-diagonal mass matrix for both charged sleptons and sneutrinos. For the charged sleptons this is a 6×6 mass matrix since there are six electroweak interaction eigenstates, $\tilde{\ell}_{L,R}$ with $\ell = e, \mu, \tau$, while for the sneutrinos the matrix is only 3×3 corresponding to the three states $\tilde{\nu}_L$ with $\nu = \nu_e, \nu_\mu, \nu_\tau$.

The non-diagonal entries in the 6×6 general matrix for charged sleptons can be described in a model-independent way in terms of a set of dimensionless parameters δ_{ij}^{AB} ($A, B = L, R$; $i, j = 1, 2, 3$, $i \neq j$), where L, R refer to the left-/right-handed SUSY partners of the corresponding leptonic degrees of freedom, and the indices i, j run over the three generations. These scenarios with general sfermion flavor mixing lead generally to larger LFV rates than in the so-called Minimal Flavor Violation Scenarios, where the mixing is induced exclusively by the Yukawa coupling of the corresponding fermion sector. This is true for both squarks

and sleptons but it is obviously of special interest in the slepton case due to the extremely small size of the lepton Yukawa couplings, suppressing LFV processes from this origin. Hence in the present case of slepton mixing we assume that the δ_{ij}^{AB} 's provide the sole source of LFV processes with potentially measurable rates.

The non-diagonal 6×6 slepton mass matrix, which we order here as $(\tilde{e}_L, \tilde{\mu}_L, \tilde{\tau}_L, \tilde{e}_R, \tilde{\mu}_R, \tilde{\tau}_R)$, is usually decomposed into left- and right-handed 3×3 blocks $M_{\tilde{\ell}, AB}^2$ as

$$\mathcal{M}_{\tilde{\ell}}^2 = \begin{pmatrix} M_{\tilde{\ell}, LL}^2 & M_{\tilde{\ell}, LR}^2 \\ M_{\tilde{\ell}, LR}^{2\dagger} & M_{\tilde{\ell}, RR}^2 \end{pmatrix}, \quad (1)$$

where

$$\begin{aligned} (M_{\tilde{\ell}, LL}^2)_{ij} &= (m_{\tilde{L}}^2)_{ij} + (m_{\ell_i}^2 + (-\frac{1}{2} + s_w^2)M_Z^2 \cos 2\beta) \delta_{ij}, \\ (M_{\tilde{\ell}, RR}^2)_{ij} &= (m_{\tilde{E}}^2)_{ij} + (m_{\ell_i}^2 - s_w^2 M_Z^2 \cos 2\beta) \delta_{ij}, \\ (M_{\tilde{\ell}, LR}^2)_{ij} &= v_1 \mathcal{A}_{ij}^\ell - m_{\ell_i} \mu \tan \beta \delta_{ij}, \end{aligned} \quad (2)$$

with flavor indexes $i, j = 1, 2, 3$, $s_w = \sqrt{1 - c_w^2}$ with $c_w = M_W/M_Z$, lepton masses $(m_{\ell_i}) = (m_e, m_\mu, m_\tau)$, and Higgsino mass parameter μ . The off-diagonal elements arise exclusively from the soft SUSY-breaking parameters: the doublet mass parameters $m_{\tilde{L}}^2$, the singlet mass parameters $m_{\tilde{E}}^2$, and the trilinear couplings \mathcal{A}^ℓ , which are all 3×3 matrices in flavor space.

The sneutrino mass matrix contains only a single 3×3 block (ordered as $(\tilde{\nu}_{eL}, \tilde{\nu}_{\mu L}, \tilde{\nu}_{\tau L})$) to start with since the singlet components are absent:

$$(\mathcal{M}_{\tilde{\nu}}^2)_{ij} = (M_{\tilde{\nu}, LL}^2)_{ij} = (m_{\tilde{L}}^2)_{ij} + \frac{1}{2} M_Z^2 \cos 2\beta \delta_{ij}. \quad (3)$$

Note that, due to $SU(2)_L$ gauge invariance, the same doublet mass parameters $m_{\tilde{L}}^2$ enter the slepton and sneutrino LL mass matrices.

If neutrino masses and neutrino flavor mixings (oscillations) were taken into account, the soft-SUSY-breaking parameters for the sneutrinos would differ from the ones for charged sleptons by a rotation with the PMNS matrix. Taking the neutrino masses and oscillations into account in the SM leads to LFV effects that are extremely small; for instance, in $\mu \rightarrow e\gamma$ they are of $\mathcal{O}(10^{-47})$ in case of Dirac neutrinos with mass around 1 eV and maximal mixing [1, 21, 22], and of $\mathcal{O}(10^{-40})$ in case of Majorana neutrinos [1, 22]. Consequently we do not expect large effects from the inclusion of neutrino mass effects here.

The dimensionless parameters δ_{ij}^{AB} allow for a unified description of the off-diagonal soft-SUSY-breaking parameters to which they are related as follows:

$$m_{\tilde{L}}^2 = \begin{pmatrix} m_{\tilde{L}_1}^2 & \delta_{12}^{LL} m_{\tilde{L}_1} m_{\tilde{L}_2} & \delta_{13}^{LL} m_{\tilde{L}_1} m_{\tilde{L}_3} \\ \delta_{21}^{LL} m_{\tilde{L}_2} m_{\tilde{L}_1} & m_{\tilde{L}_2}^2 & \delta_{23}^{LL} m_{\tilde{L}_2} m_{\tilde{L}_3} \\ \delta_{31}^{LL} m_{\tilde{L}_3} m_{\tilde{L}_1} & \delta_{32}^{LL} m_{\tilde{L}_3} m_{\tilde{L}_2} & m_{\tilde{L}_3}^2 \end{pmatrix}, \quad (4)$$

$$m_{\tilde{E}}^2 = \begin{pmatrix} m_{\tilde{E}_1}^2 & \delta_{12}^{RR} m_{\tilde{E}_1} m_{\tilde{E}_2} & \delta_{13}^{RR} m_{\tilde{E}_1} m_{\tilde{E}_3} \\ \delta_{21}^{RR} m_{\tilde{E}_2} m_{\tilde{E}_1} & m_{\tilde{E}_2}^2 & \delta_{23}^{RR} m_{\tilde{E}_2} m_{\tilde{E}_3} \\ \delta_{31}^{RR} m_{\tilde{E}_3} m_{\tilde{E}_1} & \delta_{32}^{RR} m_{\tilde{E}_3} m_{\tilde{E}_2} & m_{\tilde{E}_3}^2 \end{pmatrix}, \quad (5)$$

$$v_1 \mathcal{A}^\ell = \begin{pmatrix} m_e A_e & \delta_{12}^{LR} m_{\tilde{L}_1} m_{\tilde{E}_2} & \delta_{13}^{LR} m_{\tilde{L}_1} m_{\tilde{E}_3} \\ \delta_{21}^{LR} m_{\tilde{L}_2} m_{\tilde{E}_1} & m_\mu A_\mu & \delta_{23}^{LR} m_{\tilde{L}_2} m_{\tilde{E}_3} \\ \delta_{31}^{LR} m_{\tilde{L}_3} m_{\tilde{E}_1} & \delta_{32}^{LR} m_{\tilde{L}_3} m_{\tilde{E}_2} & m_\tau A_\tau \end{pmatrix}. \quad (6)$$

This parameterization is purely phenomenological and does not rely on any specific assumptions on the origin of the soft-SUSY-breaking parameters.

The next step is to rotate the sleptons and sneutrinos from the electroweak interaction basis into the physical mass eigenstate basis,

$$\begin{pmatrix} \tilde{\ell}_1 \\ \tilde{\ell}_2 \\ \tilde{\ell}_3 \\ \tilde{\ell}_4 \\ \tilde{\ell}_5 \\ \tilde{\ell}_6 \end{pmatrix} = R^{\tilde{\ell}} \begin{pmatrix} \tilde{e}_L \\ \tilde{\mu}_L \\ \tilde{\tau}_L \\ \tilde{e}_R \\ \tilde{\mu}_R \\ \tilde{\tau}_R \end{pmatrix}, \quad \begin{pmatrix} \tilde{\nu}_1 \\ \tilde{\nu}_2 \\ \tilde{\nu}_3 \end{pmatrix} = R^{\tilde{\nu}} \begin{pmatrix} \tilde{\nu}_{eL} \\ \tilde{\nu}_{\mu L} \\ \tilde{\nu}_{\tau L} \end{pmatrix}, \quad (7)$$

where $R^{\tilde{\ell}}$ and $R^{\tilde{\nu}}$ are the unitary matrices resulting from diagonalizing the mass matrices,

$$\begin{aligned} R^{\tilde{\ell}} \mathcal{M}_{\tilde{\ell}}^2 R^{\tilde{\ell}\dagger} &= \text{diag}\{m_{\tilde{\ell}_1}^2, m_{\tilde{\ell}_2}^2, m_{\tilde{\ell}_3}^2, m_{\tilde{\ell}_4}^2, m_{\tilde{\ell}_5}^2, m_{\tilde{\ell}_6}^2\}, \\ R^{\tilde{\nu}} \mathcal{M}_{\tilde{\nu}}^2 R^{\tilde{\nu}\dagger} &= \text{diag}\{m_{\tilde{\nu}_1}^2, m_{\tilde{\nu}_2}^2, m_{\tilde{\nu}_3}^2\}. \end{aligned} \quad (8)$$

2.2 Higgs masses and mixing

In this section we shortly review the relevant features of the MSSM Higgs sector¹ at tree-level. Unlike the SM, the MSSM requires two Higgs doublets. The Higgs potential [25]

$$\begin{aligned} V &= m_1^2 |\mathcal{H}_1|^2 + m_2^2 |\mathcal{H}_2|^2 - m_{12}^2 (\epsilon_{ab} \mathcal{H}_1^a \mathcal{H}_2^b + \text{h.c.}) + \\ &\quad \frac{1}{8} (g_1^2 + g_2^2) [|\mathcal{H}_1|^2 - |\mathcal{H}_2|^2]^2 + \frac{1}{2} g_2^2 |\mathcal{H}_1^\dagger \mathcal{H}_2|^2, \end{aligned} \quad (9)$$

contains m_1 , m_2 , m_{12} as soft-SUSY-breaking parameters; g_2, g_1 are the $SU(2)$ and $U(1)$ gauge couplings, and ϵ is the spinor metric with $\epsilon_{12} = -1$.

The doublet fields H_1 and H_2 are decomposed as

$$\begin{aligned} \mathcal{H}_1 &= \begin{pmatrix} \mathcal{H}_1^0 \\ \mathcal{H}_1^- \end{pmatrix} = \begin{pmatrix} v_1 + \frac{1}{\sqrt{2}}(\phi_1^0 - i\chi_1^0) \\ -\phi_1^- \end{pmatrix}, \\ \mathcal{H}_2 &= \begin{pmatrix} \mathcal{H}_2^+ \\ \mathcal{H}_2^0 \end{pmatrix} = \begin{pmatrix} \phi_2^+ \\ v_2 + \frac{1}{\sqrt{2}}(\phi_2^0 + i\chi_2^0) \end{pmatrix}. \end{aligned} \quad (10)$$

The Higgs potential is thus characterized at tree level by only two independent parameters: $\tan \beta = v_2/v_1$ and $M_A^2 = -m_{12}^2(\tan \beta + \cot \beta)$, where M_A is the mass of the \mathcal{CP} -odd Higgs boson A .

¹We restrict ourselves to the case of real parameters. For the case of complex parameters see Refs. [18, 24] and references therein.

The bilinear part of the Higgs potential is diagonalized by orthogonal transformations

$$\begin{pmatrix} H \\ h \end{pmatrix} = \begin{pmatrix} \cos \alpha & \sin \alpha \\ -\sin \alpha & \cos \alpha \end{pmatrix} \begin{pmatrix} \phi_1^0 \\ \phi_2^0 \end{pmatrix}, \quad (11)$$

$$\begin{pmatrix} G \\ A \end{pmatrix} = \begin{pmatrix} \cos \beta & \sin \beta \\ -\sin \beta & \cos \beta \end{pmatrix} \begin{pmatrix} \chi_1^0 \\ \chi_2^0 \end{pmatrix}, \quad (12)$$

$$\begin{pmatrix} G^\pm \\ H^\pm \end{pmatrix} = \begin{pmatrix} \cos \beta & \sin \beta \\ -\sin \beta & \cos \beta \end{pmatrix} \begin{pmatrix} \phi_1^\pm \\ \phi_2^\pm \end{pmatrix}. \quad (13)$$

where the tree-level mixing angle α is given by

$$\alpha = \arctan \left[\frac{-(M_A^2 + M_Z^2) \sin \beta \cos \beta}{M_Z^2 \cos^2 \beta + M_A^2 \sin^2 \beta - m_{h,\text{tree}}^2} \right], \quad -\frac{\pi}{2} < \alpha < 0. \quad (14)$$

The Higgs spectrum is thus:

$$\begin{aligned} & 2 \text{ neutral bosons, } \mathcal{CP} = +1 : \quad h, H, \\ & 1 \text{ neutral boson, } \mathcal{CP} = -1 : \quad A, \\ & 2 \text{ charged bosons :} \quad H^+, H^-, \\ & 3 \text{ unphysical Goldstone bosons :} \quad G, G^+, G^-. \end{aligned}$$

At tree level the neutral \mathcal{CP} -even Higgs-boson masses are determined from

$$M_{\text{Higgs}}^{2,\text{tree}} = \begin{pmatrix} M_A^2 \sin^2 \beta + M_Z^2 \cos^2 \beta & -(M_A^2 + M_Z^2) \sin \beta \cos \beta \\ -(M_A^2 + M_Z^2) \sin \beta \cos \beta & M_A^2 \cos^2 \beta + M_Z^2 \sin^2 \beta \end{pmatrix} \xrightarrow{\text{diag}} \begin{pmatrix} m_{H,\text{tree}}^2 & 0 \\ 0 & m_{h,\text{tree}}^2 \end{pmatrix}. \quad (15)$$

which yields

$$(m_{H,h}^2)_{\text{tree}} = \frac{1}{2} \left[M_A^2 + M_Z^2 \pm \sqrt{(M_A^2 + M_Z^2)^2 - 4M_Z^2 M_A^2 \cos^2 2\beta} \right] \quad (16)$$

and the charged Higgs-boson mass is given by

$$m_{H^\pm,\text{tree}}^2 = M_A^2 + M_W^2. \quad (17)$$

2.3 Calculation of higher-order corrections in the Higgs sector

We briefly review the procedure of Refs. [18, 26] for the computation of one-loop corrections to the Higgs-boson masses. The parameters appearing in the Higgs potential, Eq. (9), are renormalized as follows:

$$\begin{aligned} M_Z^2 &\rightarrow M_Z^2 + \delta M_Z^2, & T_h &\rightarrow T_h + \delta T_h, \\ M_W^2 &\rightarrow M_W^2 + \delta M_W^2, & T_H &\rightarrow T_H + \delta T_H, \\ M_{\text{Higgs}}^2 &\rightarrow M_{\text{Higgs}}^2 + \delta M_{\text{Higgs}}^2, & \tan \beta &\rightarrow \tan \beta (1 + \delta \tan \beta). \end{aligned} \quad (18)$$

M_{Higgs}^2 denotes the tree-level Higgs-boson mass matrix of Eq. (15), and T_h and T_H are the tree-level tadpoles, i.e. the terms linear in h and H in the Higgs potential.

In the \mathcal{CP} -even sector the mass and field renormalization can be set up symmetrically,

$$\delta M_{\text{Higgs}}^2 = \begin{pmatrix} \delta m_h^2 & \delta m_{hH}^2 \\ \delta m_{hH}^2 & \delta m_H^2 \end{pmatrix}, \quad \begin{pmatrix} h \\ H \end{pmatrix} \rightarrow \begin{pmatrix} 1 + \frac{1}{2}\delta Z_{hh} & \frac{1}{2}\delta Z_{hH} \\ \frac{1}{2}\delta Z_{hH} & 1 + \frac{1}{2}\delta Z_{HH} \end{pmatrix} \begin{pmatrix} h \\ H \end{pmatrix}. \quad (19)$$

The renormalized self-energies $\hat{\Sigma}(p^2)$ are expressed through the unrenormalized self-energies $\Sigma(p^2)$, the field renormalization constants, and the mass counter-terms as follows:

$$\begin{aligned} \hat{\Sigma}_{hh}(p^2) &= \Sigma_{hh}(p^2) + \delta Z_{hh}(p^2 - m_{h,\text{tree}}^2) - \delta m_h^2, \\ \hat{\Sigma}_{hH}(p^2) &= \Sigma_{hH}(p^2) + \delta Z_{hH}(p^2 - \frac{1}{2}(m_{h,\text{tree}}^2 + m_{H,\text{tree}}^2)) - \delta m_{hH}^2, \\ \hat{\Sigma}_{HH}(p^2) &= \Sigma_{HH}(p^2) + \delta Z_{HH}(p^2 - m_{H,\text{tree}}^2) - \delta m_H^2. \end{aligned} \quad (20)$$

Inserting the renormalization transformation into the Higgs mass terms gives the following Higgs-mass counter-terms:

$$\begin{aligned} \delta m_h^2 &= \delta M_A^2 \cos^2(\alpha - \beta) + \delta M_Z^2 \sin^2(\alpha + \beta) + \\ &\quad \frac{e}{2M_Z s_w c_w} (\delta T_H \cos(\alpha - \beta) \sin^2(\alpha - \beta) + \delta T_h \sin(\alpha - \beta) (1 + \cos^2(\alpha - \beta))) + \\ &\quad \delta \tan \beta \sin \beta \cos \beta (M_A^2 \sin 2(\alpha - \beta) + M_Z^2 \sin 2(\alpha + \beta)), \\ \delta m_{hH}^2 &= \frac{1}{2} (\delta M_A^2 \sin 2(\alpha - \beta) - \delta M_Z^2 \sin 2(\alpha + \beta)) + \\ &\quad \frac{e}{2M_Z s_w c_w} (\delta T_H \sin^3(\alpha - \beta) - \delta T_h \cos^3(\alpha - \beta)) - \\ &\quad \delta \tan \beta \sin \beta \cos \beta (M_A^2 \cos 2(\alpha - \beta) + M_Z^2 \cos 2(\alpha + \beta)), \\ \delta m_H^2 &= \delta M_A^2 \sin^2(\alpha - \beta) + \delta M_Z^2 \cos^2(\alpha + \beta) - \\ &\quad \frac{e}{2M_Z s_w c_w} (\delta T_H \cos(\alpha - \beta) (1 + \sin^2(\alpha - \beta)) + \delta T_h \sin(\alpha - \beta) \cos^2(\alpha - \beta)) - \\ &\quad \delta \tan \beta \sin \beta \cos \beta (M_A^2 \sin 2(\alpha - \beta) + M_Z^2 \sin 2(\alpha + \beta)). \end{aligned} \quad (21)$$

We give the Higgs doublets one renormalization constant each,

$$\mathcal{H}_1 \rightarrow (1 + \frac{1}{2}\delta Z_{\mathcal{H}_1})\mathcal{H}_1, \quad \mathcal{H}_2 \rightarrow (1 + \frac{1}{2}\delta Z_{\mathcal{H}_2})\mathcal{H}_2, \quad (22)$$

which leads to the field renormalization constants

$$\begin{aligned} \delta Z_{hh} &= \sin^2 \alpha \delta Z_{\mathcal{H}_1} + \cos^2 \alpha \delta Z_{\mathcal{H}_2}, \\ \delta Z_{hH} &= \sin \alpha \cos \alpha (\delta Z_{\mathcal{H}_2} - \delta Z_{\mathcal{H}_1}), \\ \delta Z_{HH} &= \cos^2 \alpha \delta Z_{\mathcal{H}_1} + \sin^2 \alpha \delta Z_{\mathcal{H}_2}. \end{aligned} \quad (23)$$

The counter-term for $\tan \beta$ can be expressed in terms of the vacuum expectation values as

$$\delta \tan \beta = \frac{1}{2} (\delta Z_{\mathcal{H}_2} - \delta Z_{\mathcal{H}_1}) + \frac{\delta v_2}{v_2} - \frac{\delta v_1}{v_1}, \quad (24)$$

where the δv_i are the renormalization constants of the v_i :

$$v_1 \rightarrow (1 + \delta Z_{\mathcal{H}_1}) (v_1 + \delta v_1), \quad v_2 \rightarrow (1 + \delta Z_{\mathcal{H}_2}) (v_2 + \delta v_2). \quad (25)$$

It can be shown that the divergent parts of $\delta v_1/v_1$ and $\delta v_2/v_2$ are equal [26, 27], thus we set $\delta v_2/v_2 - \delta v_1/v_1$ to zero.

In the charged Higgs sector, the renormalized self-energy is written similarly as

$$\hat{\Sigma}_{H^-H^+}(p^2) = \Sigma_{H^-H^+}(p^2) + \delta Z_{H^-H^+}(p^2 - m_{H^\pm, \text{tree}}^2) - \delta m_{H^\pm}^2, \quad (26)$$

where

$$\delta m_{H^\pm}^2 = \delta M_A^2 + \delta M_W^2, \quad (27)$$

$$\delta Z_{H^-H^+} = \sin^2 \beta \delta Z_{\mathcal{H}_1} + \cos^2 \beta \delta Z_{\mathcal{H}_2}. \quad (28)$$

We apply on-shell conditions for the masses

$$\delta M_Z^2 = \text{Re} \Sigma_{ZZ}^T(M_Z^2), \quad \delta M_W^2 = \text{Re} \Sigma_{WW}^T(M_W^2), \quad \delta M_A^2 = \text{Re} \Sigma_{AA}(M_A^2). \quad (29)$$

Since the tadpole coefficients are chosen to vanish in all orders, their counter-terms follow from $T_{\{h,H\}} + \delta T_{\{h,H\}} = 0$:

$$\delta T_h = -T_h, \quad \delta T_H = -T_H. \quad (30)$$

$\overline{\text{DR}}$ renormalization is the most convenient choice for the remaining renormalization constants

$$\delta Z_{\mathcal{H}_1} = \delta Z_{\mathcal{H}_1}^{\overline{\text{DR}}} = - [\text{Re} \Sigma'_{HH} |_{\alpha=0}]^{\text{div}},$$

$$\delta Z_{\mathcal{H}_2} = \delta Z_{\mathcal{H}_2}^{\overline{\text{DR}}} = - [\text{Re} \Sigma'_{hh} |_{\alpha=0}]^{\text{div}}, \quad (31)$$

$$\delta \tan \beta = \frac{1}{2} (\delta Z_{\mathcal{H}_2} - \delta Z_{\mathcal{H}_1}) = \delta \tan \beta^{\overline{\text{DR}}}.$$

We choose a renormalization scale of $\mu_{\overline{\text{DR}}} = m_t$ in all numerical evaluations.

Finally, in the Feynman-diagrammatic approach we are following here, the higher-order-corrected \mathcal{CP} -even Higgs-boson masses are derived by finding the poles of the (h, H) -propagator matrix. The inverse of this matrix is

$$(\Delta_{\text{Higgs}})^{-1} = -i \begin{pmatrix} p^2 - m_{H, \text{tree}}^2 + \hat{\Sigma}_{HH}(p^2) & \hat{\Sigma}_{hH}(p^2) \\ \hat{\Sigma}_{hH}(p^2) & p^2 - m_{h, \text{tree}}^2 + \hat{\Sigma}_{hh}(p^2) \end{pmatrix}. \quad (32)$$

Determining its poles is thus equivalent to solving the equation

$$\left[p^2 - m_{h, \text{tree}}^2 + \hat{\Sigma}_{hh}(p^2) \right] \left[p^2 - m_{H, \text{tree}}^2 + \hat{\Sigma}_{HH}(p^2) \right] - \left[\hat{\Sigma}_{hH}(p^2) \right]^2 = 0. \quad (33)$$

The corrected charged Higgs mass is analogously derived as the position of the pole of the charged-Higgs propagator,

$$p^2 - m_{H^\pm, \text{tree}}^2 + \hat{\Sigma}_{H^-H^+}(p^2) = 0. \quad (34)$$

We calculated the LFV contribution originating from the mixing in the slepton sector in a model-independent approach to the Higgs-boson masses. The present experimental uncertainty at the LHC for M_h , the mass of the light neutral Higgs boson, is about 350 MeV [8, 9].

This can possibly be reduced by about 50% at the LHC and below the level of ~ 50 MeV at the ILC [10]. Similarly, for the masses of the heavy neutral Higgs M_H and charged Higgs boson M_{H^\pm} , an uncertainty at the 1% level could be expected at the LHC [28]. This sets the goal for the theoretical uncertainty, which should be reduced to the same (or higher) level of accuracy.

The generic Feynman diagrams for the one-loop Higgs-boson self-energies relevant for our work are shown in Fig. 1. The diagrams were generated with FeynArts and further evaluated using FormCalc, see Sect. 2.5.

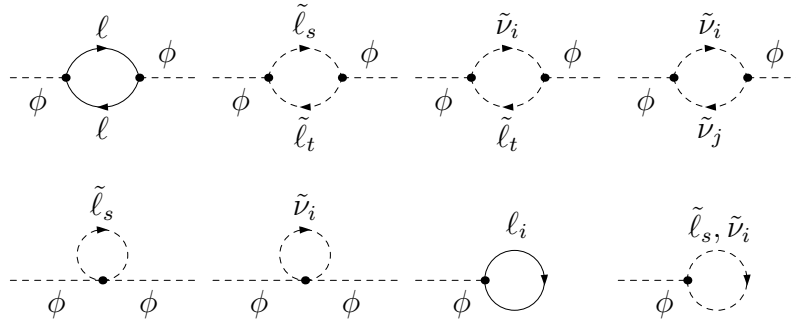


Figure 1: Generic Feynman diagrams for the Higgs-boson self-energies and tadpoles. ϕ denotes any of the Higgs bosons, h , H , A or H^\pm ; l stands for e, μ, τ ; \tilde{l}_x are the six mass eigenstates of charged sleptons, and $\tilde{\nu}_x$ are the three sneutrino states $\tilde{\nu}_e, \tilde{\nu}_\mu, \tilde{\nu}_\tau$.

2.4 Calculation of EWPO

EWPO that are known with an accuracy at the per-mille level or better have the potential to allow a discrimination between quantum effects of the SM and SUSY models, see Ref. [6] for a review. Examples are the W -boson mass M_W and the Z -boson observables, such as the effective leptonic weak mixing angle $\sin^2 \theta_{\text{eff}}$, whose present experimental uncertainties are [29]

$$\delta M_W^{\text{exp, today}} \sim 15 \text{ MeV}, \quad \delta \sin^2 \theta_{\text{eff}}^{\text{exp, today}} \sim 15 \times 10^{-5}, \quad (35)$$

The experimental uncertainty will further be reduced [30] to

$$\delta M_W^{\text{exp, future}} \sim 4 \text{ MeV}, \quad \delta \sin^2 \theta_{\text{eff}}^{\text{exp, future}} \sim 1.3 \times 10^{-5}, \quad (36)$$

at the ILC and at the GigaZ option of the ILC, respectively.

The W -boson mass can be evaluated from

$$M_W^2 \left(1 - \frac{M_W^2}{M_Z^2} \right) = \frac{\pi \alpha}{\sqrt{2} G_\mu} (1 + \Delta r) \quad (37)$$

where α is the fine-structure constant and G_μ the Fermi constant. This relation arises from comparing the prediction for muon decay with the experimentally precisely known Fermi constant. The one-loop contributions to Δr can be written as

$$\Delta r = \Delta \alpha - \frac{c_w^2}{s_w^2} \Delta \rho + (\Delta r)_{\text{rem}}, \quad (38)$$

where $\Delta\alpha$ is the shift in the fine-structure constant due to the light fermions of the SM, $\Delta\alpha \propto \log(M_Z/m_f)$, and $\Delta\rho$ is the leading contribution to the ρ parameter [31] from (certain) fermion and sfermion loops. The remainder part $(\Delta r)_{\text{rem}}$ contains in particular the contributions from the Higgs sector.

The effective leptonic weak mixing angle at the Z -boson resonance, $\sin^2\theta_{\text{eff}}$, is defined through the vector and axial-vector couplings (g_V^ℓ and g_A^ℓ) of leptons (ℓ) to the Z boson, measured at the Z -boson pole. If this vertex is written as $i\bar{\ell}\gamma^\mu(g_V^\ell - g_A^\ell\gamma_5)\ell Z_\mu$ then

$$\sin^2\theta_{\text{eff}} = \frac{1}{4} \left(1 - \text{Re} \frac{g_V^\ell}{g_A^\ell} \right). \quad (39)$$

At tree level this coincides with the sine of the weak mixing angle, $\sin^2\theta_W = 1 - M_W^2/M_Z^2$, in the on-shell scheme. Loop corrections enter through higher-order contributions to g_V^ℓ and g_A^ℓ .

Both of these (pseudo-)observables are affected by shifts in the quantity $\Delta\rho$ according to

$$\Delta M_W \approx \frac{M_W}{2} \frac{c_w^2}{c_w^2 - s_w^2} \Delta\rho, \quad \Delta \sin^2\theta_{\text{eff}} \approx -\frac{c_w^2 s_w^2}{c_w^2 - s_w^2} \Delta\rho. \quad (40)$$

The quantity $\Delta\rho$ is defined by the relation

$$\Delta\rho = \frac{\Sigma_Z^T(0)}{M_Z^2} - \frac{\Sigma_W^T(0)}{M_W^2} \quad (41)$$

with the unrenormalized transverse parts of the Z - and W -boson self-energies at zero momentum, $\Sigma_{Z,W}^T(0)$. It represents the leading universal corrections to the electroweak precision observables induced by mass splitting between partners in isospin doublets [31]. Consequently, it is sensitive to the mass-splitting effects induced by non-minimal flavour mixing.

Beyond the $\Delta\rho$ approximation, the shifts in M_W and $\sin^2\theta_{\text{eff}}$ originate from the complete sfermion contributions to the quantity Δr and to other combinations of the various vector-boson self-energies. It has been numerically verified that $\Delta\rho$ yields an excellent approximation for the full calculation in the case of NMFV effects [6, 7], however.

We calculated the LFV contribution to the above-mentioned observables entering the Z - and W -boson self-energies at the one-loop level through the ρ -parameter. The generic Feynman diagrams contributing to our calculation are shown in Fig. 2. The diagrams were generated with FeynArts and further evaluated using FormCalc, see Sect. 2.5. The resulting evaluation of $\Delta\rho$ has been made publicly available in FeynHiggs. Using Eq. (40) the shifts in M_W and $\sin^2\theta_{\text{eff}}$ induced by LFV have been evaluated, see Sect. 4.

2.5 Changes in FeynArts, FormCalc, and FeynHiggs

FeynArts [11] and FormCalc [14] provide a high level of automation for perturbative calculations up to one loop. This is particularly important for models with a large particle content such as the MSSM [12]. Here we briefly describe the recent extension of the implementation of the MSSM in these packages to include LFV. Details on the previous inclusion of NMFV can be found in Refs. [11, 37]. This involves firstly the modification of the slepton couplings

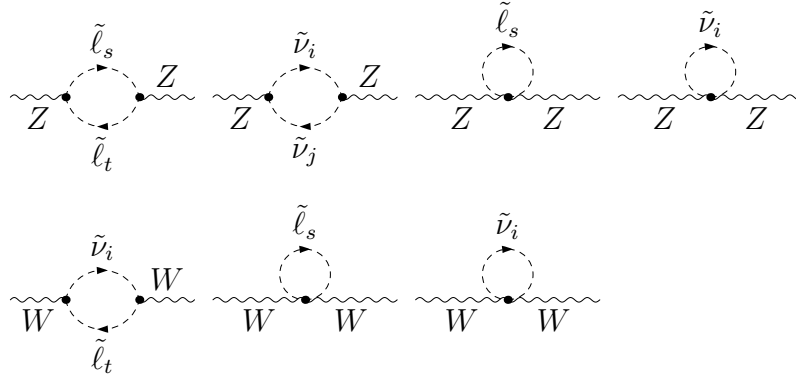


Figure 2: Generic Feynman diagrams for the W - and Z -boson self-energies containing sleptons in loops. The six mass eigenstates of charged sleptons are denoted by $\tilde{\ell}_x$, and $\tilde{\nu}_x$ stands for the three sneutrino states $\tilde{\nu}_e, \tilde{\nu}_\mu, \tilde{\nu}_\tau$.

in the existing FeynArts model file for the MSSM and secondly the corresponding initialization routines for the slepton masses and mixings, i.e. the 6×6 and 3×3 diagonalization of the mass matrices in FormCalc.

2.5.1 FeynArts Model File

FeynArts' add-on model file `FV.mod` applies algebraic substitutions to the Feynman rules of `MSSM.mod` to upgrade minimal to non-minimal flavor mixing in the sfermion sector. The original version modified only the squark sector, i.e. NMFV, and needed to be generalized to include LFV. We solved this by allowing the user to choose which sfermion types to introduce non-minimal mixing for through the variable `$FV` (set before model initialization, of course). For example,

```
$FV = {11, 12, 13, 14};
InsertFields[... , Model -> {MSSM, FV}]
```

sets non-minimal mixing for all four sfermion types, with $11 = \tilde{\nu}$, $12 = \tilde{\ell}$, $13 = \tilde{u}$, and $14 = \tilde{d}$ as usual in `MSSM.mod`. For compatibility with the old NMFV-only version, the default is `$FV = {13, 14}`.

`FV.mod` introduces the following new quantities:

<code>UASf</code> [s_1, s_2, t]	the slepton mixing matrix R , where $s_1, s_2 = 1 \dots 6$, $t = 1 (\tilde{\nu}), 2 (\tilde{\ell}), 3 (\tilde{u}), 4 (\tilde{d})$,
<code>MASf</code> [s, t]	the slepton masses, where $s = 1 \dots 6$, $t = 1 (\tilde{\nu}), 2 (\tilde{\ell}), 3 (\tilde{u}), 4 (\tilde{d})$.

Entries $4 \dots 6$ are unused for the sneutrino.

2.5.2 Model Initialization in FormCalc

The initialization of the generalized slepton-mixing parameters `MASf` and `UASf` is already built into FormCalc's regular MSSM model-initialization file `model_mssm.F` but not turned on by default. It must be enabled by adjusting the FV preprocessor flag in `run.F`:

```
#define FV 2
```

where 2 is the lowest sfermion type t for which flavor violation is enabled, i.e. $\tilde{\ell}$.

The flavor-violating parameters δ_{ij}^{AB} are represented in FormCalc by the `deltaSf` matrix:

```
double complex deltaSf(s1,s2,t)  the matrix ( $\delta_t$ )s1s2, where
                                     s1, s2 = 1...6 (1...3 for  $\tilde{\nu}$ ),
                                     t = 2 ( $\tilde{\ell}$ ), 3 ( $\tilde{u}$ ), 4 ( $\tilde{d}$ ).
```

Since δ is an Hermitian matrix, only the entries above the diagonal are considered. The δ_{ij}^{AB} are located at the following places in the matrix δ :

$$\left(\begin{array}{ccc|ccc} \cdot & \delta_{12}^{LL} & \delta_{13}^{LL} & \cdot & \delta_{12}^{LR} & \delta_{13}^{LR} \\ \cdot & \cdot & \delta_{23}^{LL} & \delta_{12}^{RL*} & \cdot & \delta_{23}^{LR} \\ \cdot & \cdot & \cdot & \delta_{13}^{RL*} & \delta_{23}^{RL*} & \cdot \\ \hline \cdot & \cdot & \cdot & \cdot & \delta_{12}^{RR} & \delta_{13}^{RR} \\ \cdot & \cdot & \cdot & \cdot & \cdot & \delta_{23}^{RR} \\ \cdot & \cdot & \cdot & \cdot & \cdot & \cdot \end{array} \right)$$

The trilinear couplings A_f acquire non-zero off-diagonal entries in the presence of LFV through the relations

$$m_{f,i}(A_f)_{ij} = (M_{f,LR}^2)_{ij}, \quad i, j = 1 \dots 3, \quad (42)$$

see Eq. (2). These off-diagonal trilinear couplings (and hence the δ 's) appear directly in the Higgs–slepton–slepton couplings, whereas all other effects are mediated through the masses and mixings.

The described changes are contained in FeynArts 3.9 and FormCalc 8.4, which are publicly available from `feynarts.de`.

2.5.3 Inclusion of LFV into FeynHiggs

As discussed above, the new corrections to the (renormalized) Higgs-boson self-energies (and thus to the Higgs-boson masses), as well as to $\Delta\rho$ (and thus to M_W and $\sin^2\theta_{\text{eff}}$) have been included in FeynHiggs [15–19].

The corrections are activated by setting one or more of the δ_{ij}^{AB} to non-zero values. All δ_{ij}^{AB} that are not set are assumed to be zero. The non-zero value can be set in three ways:

- by including them in the input file, e.g.

```
deltaLLL23    0.1
```

where the general format of the identifier is

```
deltaFXYij, F = L,E,Q,U,D, XY = LL,LR,RL,RR, ij = 12,23,13
```

- by calling the subroutine `FHSetLFV(...)` from your Fortran/C/C++ code.
- by calling the routine `FHSetLFV[...]` from your Mathematica code.

The detailed invocation of `FHSetLFV` is given in the corresponding man page included in the FeynHiggs distribution. The LFV corrections are included starting from FeynHiggs version 2.10.2, available from `feynhiggs.de`.

3 Selection of Input Parameters

3.1 MSSM scenarios

For the following numerical analysis we chose the MSSM parameter sets of Ref. [20]. This framework contains six specific points S1...S6 in the MSSM parameter space, all of which are well compatible with present data, including recent LHC searches and the measurements of the muon anomalous magnetic moment. The values of the various MSSM parameters as well as the values of the predicted MSSM mass spectra are summarized in Tab. 1. They were evaluated with the program FeynHiggs [15–19].

For simplicity, and to reduce the number of independent MSSM input parameters, we assume equal soft masses for the sleptons of the first and second generations (similarly for the squarks), and for the left and right slepton sectors (similarly for the squarks). We choose equal trilinear couplings for the stop and sbottom squarks and for the sleptons consider only the stau trilinear coupling; the others are set to zero. We assume an approximate GUT relation for the gaugino soft-SUSY-breaking parameters. The pseudoscalar Higgs mass M_A and the μ parameter are taken as independent input parameters. In summary, the six points S1...S6 are defined in terms of the following subset of ten input MSSM parameters:

$$\begin{array}{lll}
 m_{\tilde{L}_1} = m_{\tilde{L}_2}, & m_{\tilde{L}_3}, & \text{(with } m_{\tilde{L}_i} = m_{\tilde{E}_i}, i = 1, 2, 3) \\
 m_{\tilde{Q}_1} = m_{\tilde{Q}_2} & m_{\tilde{Q}_3}, & \text{(with } m_{\tilde{Q}_i} = m_{\tilde{U}_i} = m_{\tilde{D}_i}, i = 1, 2, 3) \\
 A_t = A_b, & A_\tau, & \\
 M_2 = 2M_1 = M_3/4, & \mu, & \\
 M_A, & \tan \beta. &
 \end{array}$$

The specific values of these ten MSSM parameters in Tab. 1 are chosen to provide different patterns in the various sparticle masses, but all leading to rather heavy spectra and thus naturally in agreement with the absence of SUSY signals at the LHC. In particular, all points lead to rather heavy squarks and gluinos above 1200 GeV and heavy sleptons above 500 GeV (where the LHC limits would also permit substantially lighter sleptons). The values of M_A within the interval (500, 1500) GeV, $\tan \beta$ within the interval (10, 50) and a large A_t within (1000, 2500) GeV are fixed such that a light Higgs boson h within the LHC-favoured range (123, 127) GeV is obtained.

The large values of $M_A \geq 500$ GeV place the Higgs sector of our scenarios in the so-called decoupling regime [32], where the couplings of h to gauge bosons and fermions are close to the SM Higgs couplings, and the heavy H couples like the pseudoscalar A , and all heavy Higgs bosons are close in mass. With increasing M_A , the heavy Higgs bosons tend

Table 1: Selected points in the MSSM parameter space (upper part) and their corresponding spectra (lower part). All dimensionful quantities are in GeV.

	S1	S2	S3	S4	S5	S6
$m_{\tilde{L}_{1,2}}$	500	750	1000	800	500	1500
$m_{\tilde{L}_3}$	500	750	1000	500	500	1500
M_2	500	500	500	500	750	300
A_τ	500	750	1000	500	0	1500
μ	400	400	400	400	800	300
$\tan\beta$	20	30	50	40	10	40
M_A	500	1000	1000	1000	1000	1500
$m_{\tilde{Q}_{1,2}}$	2000	2000	2000	2000	2500	1500
$m_{\tilde{Q}_3}$	2000	2000	2000	500	2500	1500
A_t	2300	2300	2300	1000	2500	1500
$m_{\tilde{\ell}_{1\dots 6}}$	489–515	738–765	984–1018	474–802	488–516	1494–1507
$m_{\tilde{\nu}_{1\dots 3}}$	496	747	998	496–797	496	1499
$m_{\tilde{\chi}_{1,2}^\pm}$	375–531	376–530	377–530	377–530	710–844	247–363
$m_{\tilde{\chi}_{1,2}^0}$	244–531	245–531	245–530	245–530	373–844	145–363
M_h	126.6	127.0	127.3	123.1	123.8	125.1
M_H	500	1000	999	1001	1000	1499
M_A	500	1000	1000	1000	1000	1500
M_{H^\pm}	507	1003	1003	1005	1003	1502
$m_{\tilde{u}_{1\dots 6}}$	1909–2100	1909–2100	1908–2100	336–2000	2423–2585	1423–1589
$m_{\tilde{d}_{1\dots 6}}$	1997–2004	1994–2007	1990–2011	474–2001	2498–2503	1492–1509
$m_{\tilde{g}}$	2000	2000	2000	2000	3000	1200

to decouple from low-energy physics and the light h behaves like H_{SM} . This type of MSSM Higgs sector seems to be in good agreement with recent LHC data [33]. We checked with the code HiggsBounds [34] that this is indeed the case (although S3 is right ‘at the border’).

Particularly, the absence of gluinos at the LHC so far forbids too low M_3 and, through the assumed GUT relation, also a too low M_2 . This is reflected by our choice of M_2 and μ which give gaugino masses compatible with present LHC bounds. Finally, we required that all our points lead to a prediction of the anomalous magnetic moment of the muon in the MSSM that can fill the present discrepancy between the Standard Model prediction and the experimental value.

3.2 Selection of δ_{ij}^{AB} mixings

Finally, we need to set the range of values for the explored δ_{ij}^{AB} ’s. We use the constraints of Ref. [20], calculated from the following LFV processes:

1. Radiative LFV decays: $\mu \rightarrow e\gamma$, $\tau \rightarrow e\gamma$, and $\tau \rightarrow \mu\gamma$. These are sensitive to the δ_{ij}^{AB} ’s via the $(\ell_i \ell_j \gamma)_{1\text{-loop}}$ vertices with a real photon.
2. Leptonic LFV decays: $\mu \rightarrow 3e$, $\tau \rightarrow 3e$, and $\tau \rightarrow 3\mu$. These are sensitive to the δ_{ij}^{AB} ’s

via the $(\ell_i \ell_j \gamma)_{1\text{-loop}}$ vertices with a virtual photon, via the $(\ell_i \ell_j Z)_{1\text{-loop}}$ vertices with a virtual Z , and via the $(\ell_i \ell_j h)_{1\text{-loop}}$, $(\ell_i \ell_j H)_{1\text{-loop}}$ and $(\ell_i \ell_j A)_{1\text{-loop}}$ vertices with virtual Higgs bosons.

3. Semileptonic LFV tau decays: $\tau \rightarrow \mu \eta$ and $\tau \rightarrow e \eta$. These are sensitive to the δ_{ij}^{AB} 's via the $(\tau \ell A)_{1\text{-loop}}$ vertex with a virtual A and the $(\tau \ell Z)_{1\text{-loop}}$ vertex with a virtual Z , where $\ell = \mu, e$, respectively.
4. Conversion of μ into e in heavy nuclei: These are sensitive to the δ_{ij}^{AB} 's via the $(\mu e \gamma)_{1\text{-loop}}$ vertex with a virtual photon, the $(\mu e Z)_{1\text{-loop}}$ vertex with a virtual Z , and the $(\mu e h)_{1\text{-loop}}$ and $(\mu e H)_{1\text{-loop}}$ vertices with a virtual Higgs boson.

Table 2: Present upper bounds on the slepton mixing parameters $|\delta_{ij}^{AB}|$ for the MSSM points S1...S6 defined in Tab. 1. The bounds for $|\delta_{ij}^{RL}|$ are similar to those of $|\delta_{ij}^{LR}|$.

	S1	S2	S3	S4	S5	S6
$ \delta_{12}^{LL} _{\max}$	10×10^{-5}	7.5×10^{-5}	5×10^{-5}	6×10^{-5}	42×10^{-5}	8×10^{-5}
$ \delta_{12}^{LR} _{\max}$	2×10^{-6}	3×10^{-6}	4×10^{-6}	3×10^{-6}	2×10^{-6}	1.2×10^{-5}
$ \delta_{12}^{RR} _{\max}$	1.5×10^{-3}	1.2×10^{-3}	1.1×10^{-3}	1×10^{-3}	2×10^{-3}	5.2×10^{-3}
$ \delta_{13}^{LL} _{\max}$	5×10^{-2}	5×10^{-2}	3×10^{-2}	3×10^{-2}	23×10^{-2}	5×10^{-2}
$ \delta_{13}^{LR} _{\max}$	2×10^{-2}	3×10^{-2}	4×10^{-2}	2.5×10^{-2}	2×10^{-2}	11×10^{-2}
$ \delta_{13}^{RR} _{\max}$	5.4×10^{-1}	5×10^{-1}	4.8×10^{-1}	5.3×10^{-1}	7.7×10^{-1}	7.7×10^{-1}
$ \delta_{23}^{LL} _{\max}$	6×10^{-2}	6×10^{-2}	4×10^{-2}	4×10^{-2}	27×10^{-2}	6×10^{-2}
$ \delta_{23}^{LR} _{\max}$	2×10^{-2}	3×10^{-2}	4×10^{-2}	3×10^{-2}	2×10^{-2}	12×10^{-2}
$ \delta_{23}^{RR} _{\max}$	5.7×10^{-1}	5.2×10^{-1}	5×10^{-1}	5.6×10^{-1}	8.3×10^{-1}	8×10^{-1}

Applying the most recent constraints from the LFV processes listed above yields up-to-date limits on the δ_{ij}^{AB} [20]. Using these upper bounds on δ_{ij}^{AB} given in Tab. 2, we calculate the

corrections to the Higgs boson masses and the EWPO. For each explored non-vanishing delta, the corresponding physical sfermion masses and mixings, as well as the EWPO and Higgs masses were numerically computed with FeynHiggs 2.10.2, which includes the analytical results of our calculations.

4 Results and discussion

We implemented the full one-loop results including all LFV mixing terms for the W -, Z -, and Higgs-boson self-energies in FeynHiggs 2.10.2. The analytical results are lengthy and not shown here. For the numerical study we analyzed all 12 δ_{ij}^{AB} for the MSSM scenarios defined in Tab. 1. For a better view of the LFV effects we shall plot only the differences

$$\Delta\rho^{\text{LFV}} = \Delta\rho - \Delta\rho^{\text{MSSM}}, \quad (43)$$

$$\delta M_W^{\text{LFV}} = M_W - M_W^{\text{MSSM}}, \quad (44)$$

$$\delta \sin^2 \theta_{\text{eff}}^{\text{LFV}} = \sin^2 \theta_{\text{eff}} - \sin^2 \theta_{\text{eff}}^{\text{MSSM}}, \quad (45)$$

where $\Delta\rho^{\text{MSSM}}$, M_W^{MSSM} , and $\sin^2 \theta_{\text{eff}}^{\text{MSSM}}$ are the values with $\delta_{ij}^{AB} = 0$ (the latter two evaluated with the help of Eq. (40)). Furthermore we use

$$\Delta M_h^{\text{LFV}} = M_h - M_h^{\text{MSSM}}, \quad (46)$$

$$\Delta M_H^{\text{LFV}} = M_H - M_H^{\text{MSSM}}, \quad (47)$$

$$\Delta M_{H^\pm}^{\text{LFV}} = M_{H^\pm} - M_{H^\pm}^{\text{MSSM}}, \quad (48)$$

where again M_h^{MSSM} , M_H^{MSSM} and $M_{H^\pm}^{\text{MSSM}}$ are the values for $\delta_{ij}^{AB} = 0$. The SM results for M_W and $\sin^2 \theta_{\text{eff}}$ are $M_W = 80.361$ GeV and $\sin^2 \theta_{\text{eff}} = 0.23152$ as evaluated with FeynHiggs (using the approximation formulas given in Refs. [35,36]). The numerical values of $\Delta\rho$, M_W , $\sin^2 \theta_{\text{eff}}$, M_h , M_H and M_{H^\pm} in the MSSM with all $\delta_{ij}^{AB} = 0$ are summarized in Tab. 3.

Our numerical results are shown in Figs. 3–10. The six plots in each figure are ordered as follows. Upper left: $\Delta\rho^{\text{LFV}}$, upper right: δM_W^{LFV} , middle left: $\delta \sin^2 \theta_{\text{eff}}^{\text{LFV}}$, middle right: ΔM_h^{LFV} , lower left: ΔM_H^{LFV} , and lower right: $\Delta M_{H^\pm}^{\text{LFV}}$, as a function of δ_{13}^{LL} (Fig. 3), δ_{23}^{LL} (Fig. 4), δ_{13}^{LR} (Fig. 5), δ_{23}^{LR} (Fig. 6), δ_{13}^{RL} (Fig. 7), δ_{23}^{RL} (Fig. 8), δ_{13}^{RR} (Fig. 9) and δ_{23}^{RR} (Fig.10). The legends are shown only in the first plot of each figure. We do not show results for LFV effects involving only the first and second generation. While they are included for completeness in our analytical results, they are expected to have a negligible effect on the observables considered here. The latter is confirmed by the numerical analysis presented in the next subsections.

4.1 EWPO

We start with the investigation of the LFV effects on the electroweak precision observables. Experimental bounds on the δ_{12}^{AB} are very strict (see Tab. 2) and hence it does not contribute sizably. The bounds on the other δ_{ij}^{AB} 's are less strict but in most cases we still do not get appreciable contributions to the EWPO (but now can quantify their corresponding sizes). The only significant contribution comes from δ_{23}^{LL} . The upper left plot in Fig. 4 shows our

	S1	S2	S3	S4	S5	S6
$\Delta\rho$	2.66×10^{-5}	1.72×10^{-5}	1.39×10^{-5}	2.35×10^{-4}	2.36×10^{-5}	2.14×10^{-5}
M_W	80.362	80.362	80.361	80.375	80.364	80.363
$\sin^2 \theta_{\text{eff}}$	0.23151	0.23152	0.23152	0.23143	0.23150	0.23151
M_h	126.257	126.629	126.916	123.205	123.220	124.695
M_H	500.187	999.580	999.206	1001.428	1000.239	1499.365
M_{H^\pm}	506.888	1003.182	1003.005	1005.605	1003.454	1501.553

Table 3: The values of $\Delta\rho$, M_W , $\sin^2 \theta_{\text{eff}}$, M_h , M_H and M_{H^\pm} for the selected S1-S6 MSSM points defined in Tab. 1 (i.e. with all $\delta_{ij}^{AB} = 0$). Mass values are in GeV.

results for $\Delta\rho$ as functions of δ_{23}^{LL} under the presently allowed experimental range given in Tab. 2. Depending on the choice of scenario (S1...S6), values of $\mathcal{O}(10^{-3})$ can be reached. The largest values are found in S5, where the values of δ_{23}^{LL} of up to ± 0.3 are permitted. For the same value of δ_{23}^{LL} we find the largest contributions in S6, which possesses the relatively largest values of soft-SUSY-breaking parameters in the slepton sector. This indicates that in general large contributions to the EWPO are possible as soon as heavy sleptons are involved. Conversely, while such heavy sleptons are in general difficult to detect directly at the LHC or the ILC, their presence could be visible in case of large LFV contributions via a shift in the EWPO.

Turning to the (pseudo-)observables M_W and $\sin^2 \theta_{\text{eff}}$, respectively shown in the upper right and middle left plot of Fig. 4, we can compare the size of the LFV contributions to the current and future anticipated accuracies in these observables. The black line in both plots indicates the result for $\delta_{23}^{LL} = 0$. The red line shows the current level of accuracy, Eq. (35), while the blue line indicates the future ILC/GigaZ precision, Eq. (36). We refrain from putting the absolute values of these observables since their values strongly depend on the choice of the stop/sbottom sector (see Ref. [6] and references therein), which is independent on the slepton sector under investigation here. While the current level of accuracy only has the potential to restrict δ_{23}^{LL} in S5 and S6, the future accuracy (particularly in $\sin^2 \theta_{\text{eff}}$) can set stringent bounds in all six scenarios.

The overall conclusion for the EWPO is that, while δ_{23}^{LL} is the most difficult one to restrict using ‘conventional’ LFV observables (see Sect. 3.2), it has (by far) the strongest impact

on EWPO. Depending on the stop/sbottom sector, new bounds beyond the ‘conventional’ LFV observables can be obtained even with the current precision, and still better with the (anticipated) future accuracies.

4.2 Higgs masses

We now turn to the effects of the LFV contributions on the prediction of the neutral \mathcal{CP} -even and the charged MSSM Higgs-boson masses. As discussed in Sect. 2.3, the theoretical accuracy should reach a precision of ~ 50 MeV in the case of M_h and about $\sim 1\%$ in the case of the heavy Higgs bosons. The calculation of M_h in the presence of non-minimal flavor violation (NMFV) in the squark sector [5] indicated that corrections as large as $\mathcal{O}(10$ GeV) are possible (for the NMFV δ_{ij}^{AB} in agreement with all other precision data). Similar or even larger corrections were found for the heavy Higgs bosons, in particular for the charged Higgs boson. Large corrections were associated especially with non-zero values of $\delta_{23}^{LR,RL}$.

Even though the corrections from the slepton sector are naturally much smaller than from the squark sector, the LFV contributions could be expected to exceed future and possibly even current experimental uncertainties. Indeed, the estimated theoretical uncertainties for the LFV contributions of at least $\mathcal{O}(100$ MeV) for M_h and $\mathcal{O}(10$ GeV) for M_{H^\pm} were at the level of or exceeding the future anticipated accuracies. Thus, the LFV had to be evaluated and analyzed in order to reach the required level of precision.

The Higgs-boson masses are shown in the middle right plot (M_h), the lower left (M_H) and the lower right plot (M_{H^\pm}) of each figure. As expected from the NMFV analysis in the squark sector [5], the largest effects are found for $\delta_{23}^{LR,RL}$, but similarly for $\delta_{13}^{LR,RL}$, indicating that only the electroweak, not the Yukawa couplings, play a relevant role in these corrections. Contrary to expectations, the corrections to M_h *always* stay below the level of a few MeV. Though this result obviates the above-mentioned uncertainty of $\mathcal{O}(100$ MeV), these contributions are too small to yield a sizable numerical effect.

Turning to the heavy Higgs bosons, the contributions to M_H (most sizable again for $\delta_{23,13}^{LR,RL}$) do not exceed $\mathcal{O}(100$ MeV) and are thus effectively negligible. Substantially larger corrections are found, in agreement with the expectations from Ref. [5] for the charged Higgs-boson mass. They can reach the level of nearly -2 GeV, see Figs. 5–8. For the chosen values of M_A (or M_{H^\pm}) this stays below the level of 1%. The absolute size of the corrections is not connected to the value of M_{H^\pm} in S1...S6, however. Choosing starting values of M_A somewhat smaller (requiring a new evaluation of the corresponding bounds on the LFV δ_{ij}^{AB}), could yield relative corrections to M_{H^\pm} at the level of 1%. Furthermore, as in the case of the light Higgs-boson mass, the explicit calculation of the LFV effects eliminates the theory uncertainty associated to these effects, thus improving the theoretical accuracy.

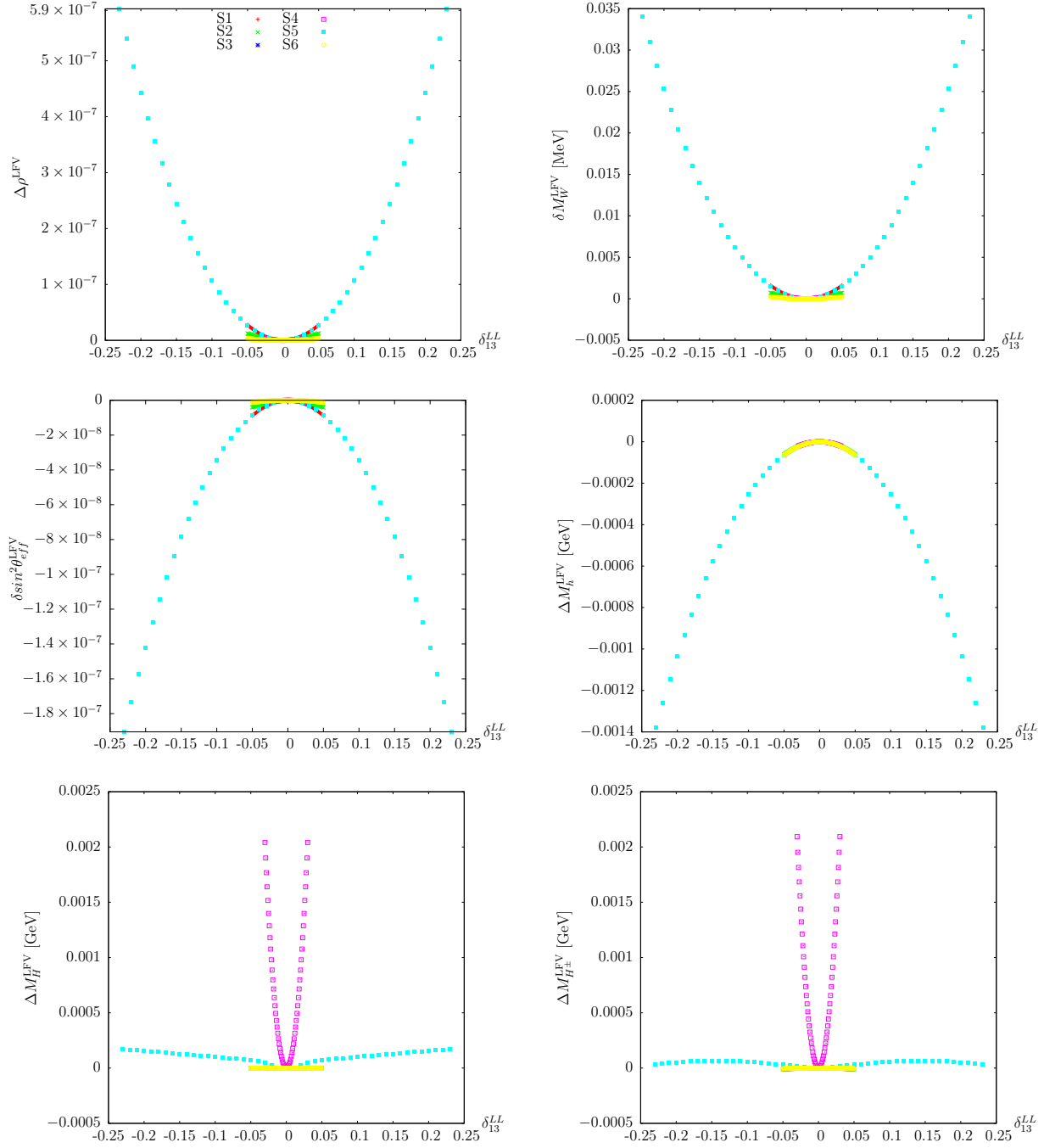


Figure 3: EWPO and Higgs masses as a function of slepton mixing δ_{13}^{LL} for the six points defined in the Tab. 1.

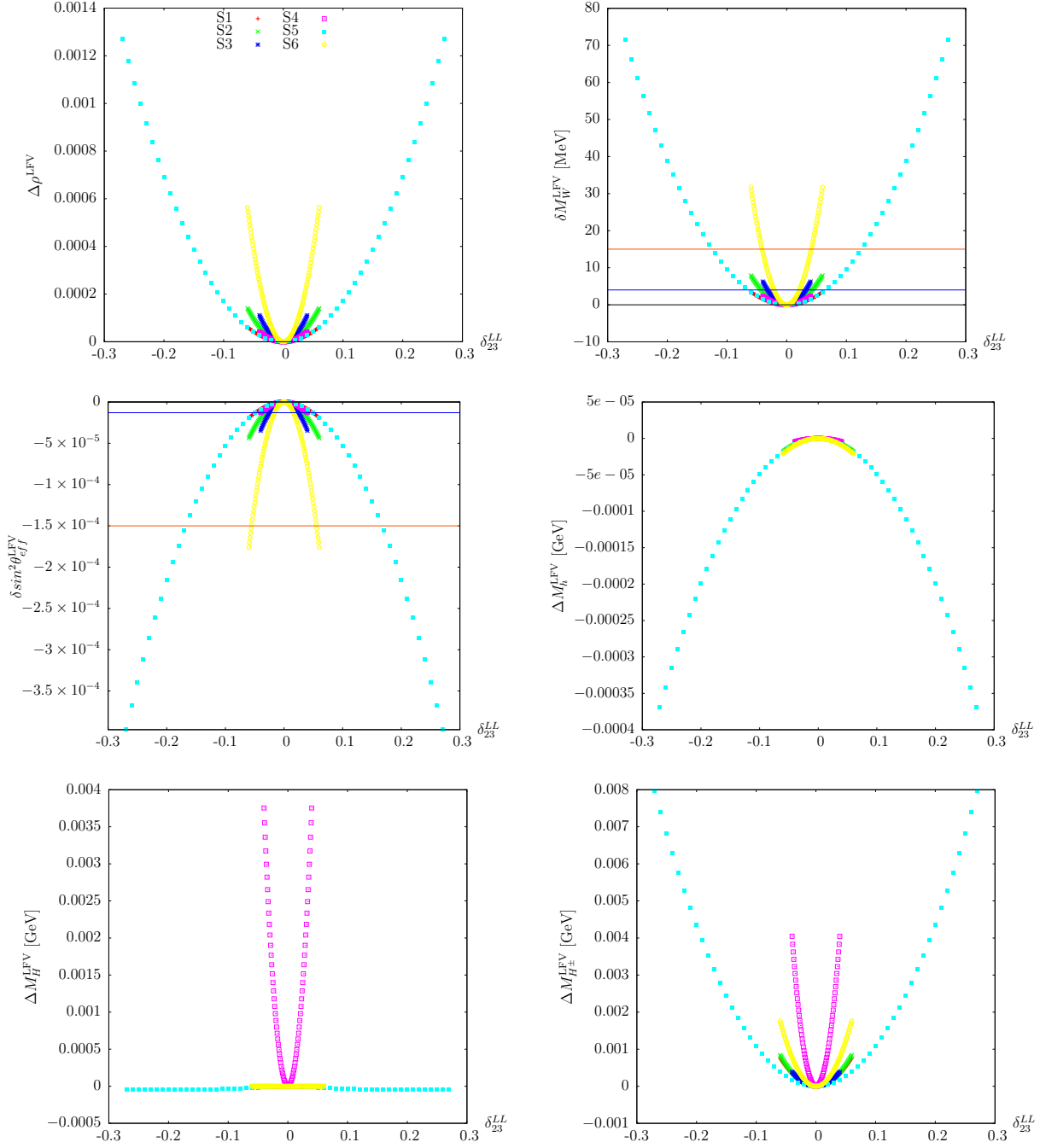


Figure 4: EWPO and Higgs masses as a function of slepton mixing δ_{23}^{LL} for the six points defined in the Tab. 1. Solid red (blue) line shows the present (future) experimental uncertainty.

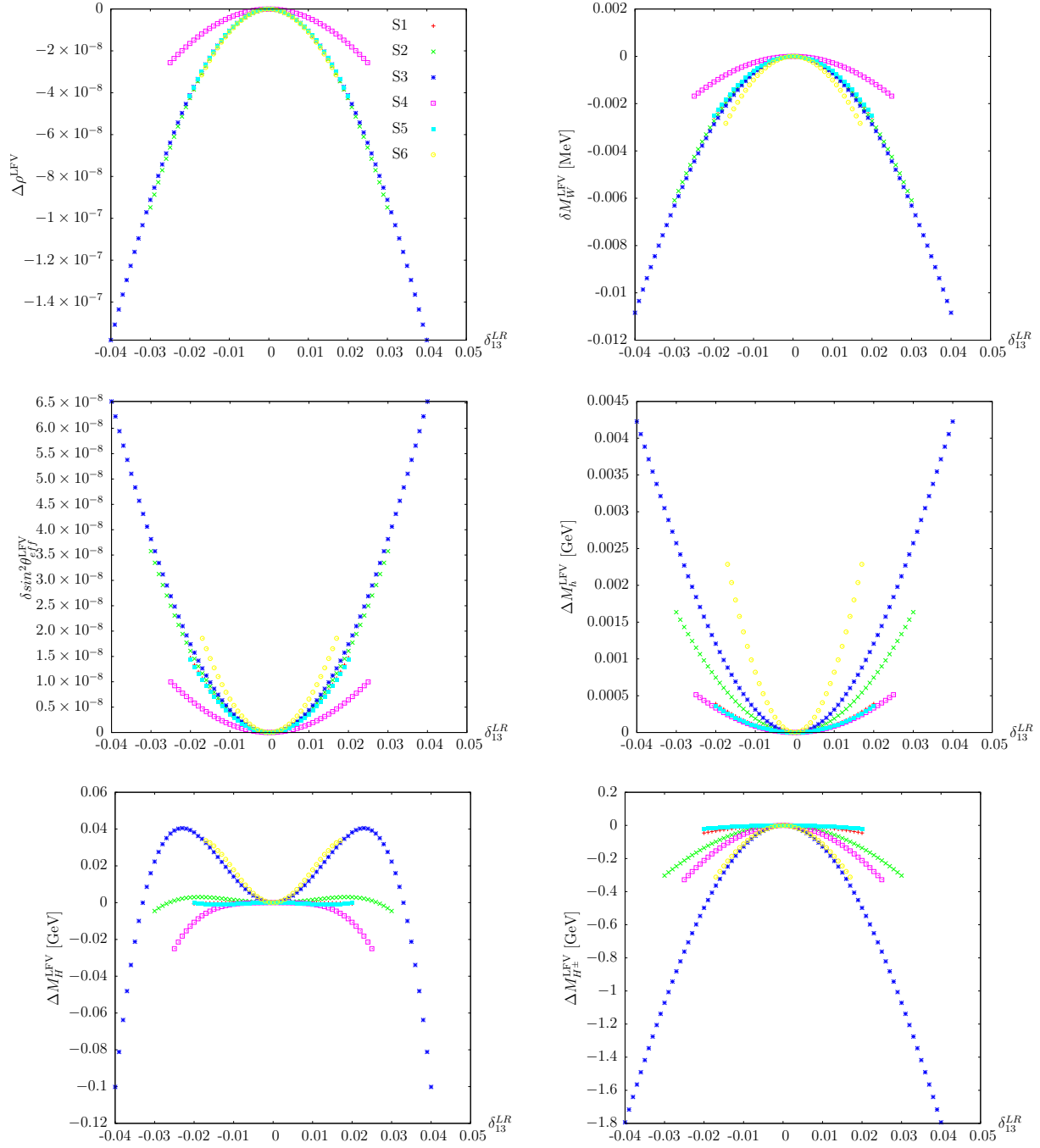


Figure 5: EWPO and Higgs masses as a function of slepton mixing δ_{13}^{LR} for the six points defined in the Tab. 1.

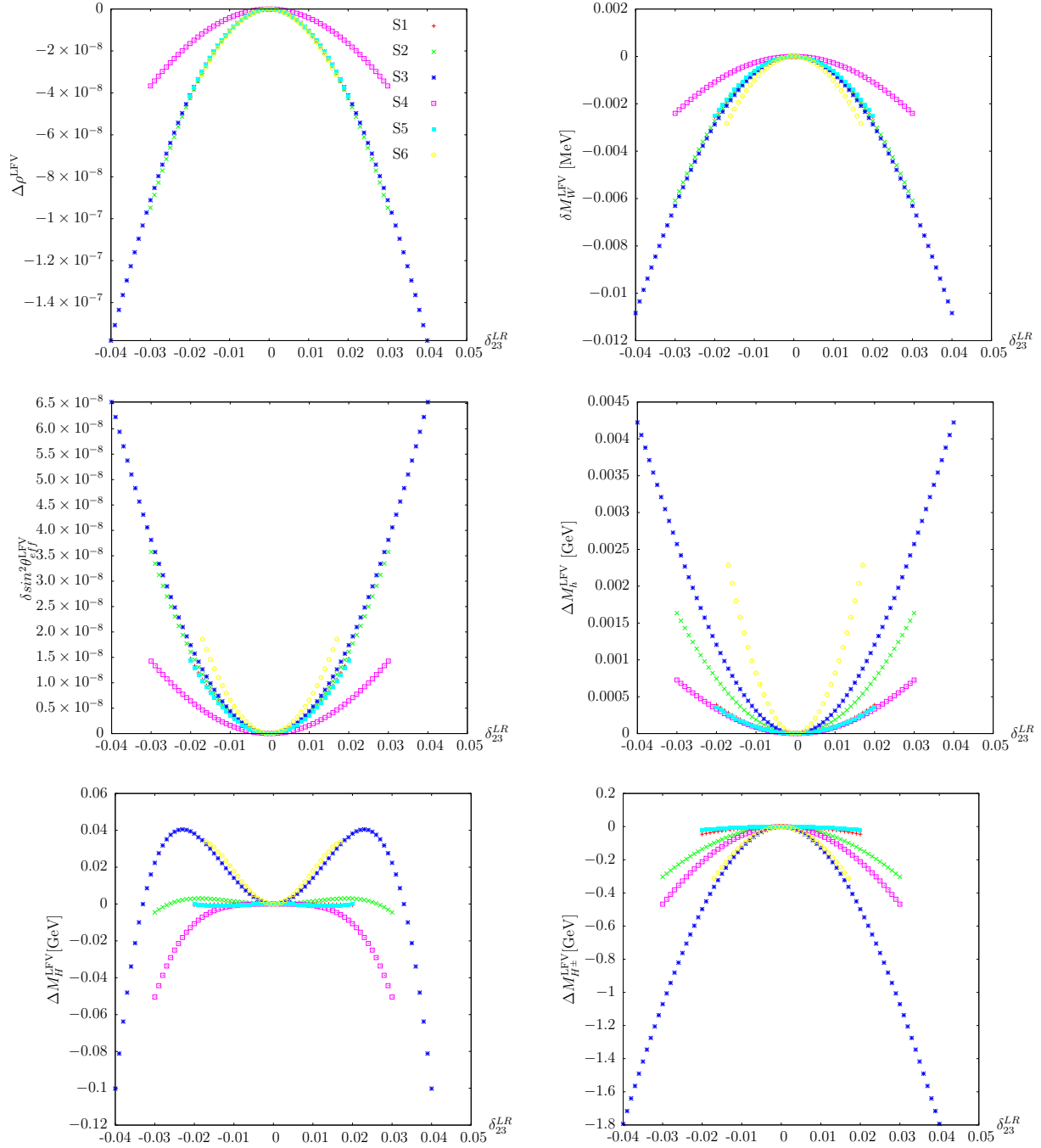


Figure 6: EWPO and Higgs masses as a function of slepton mixing δ_{23}^{LR} for the six points defined in the Tab. 1.

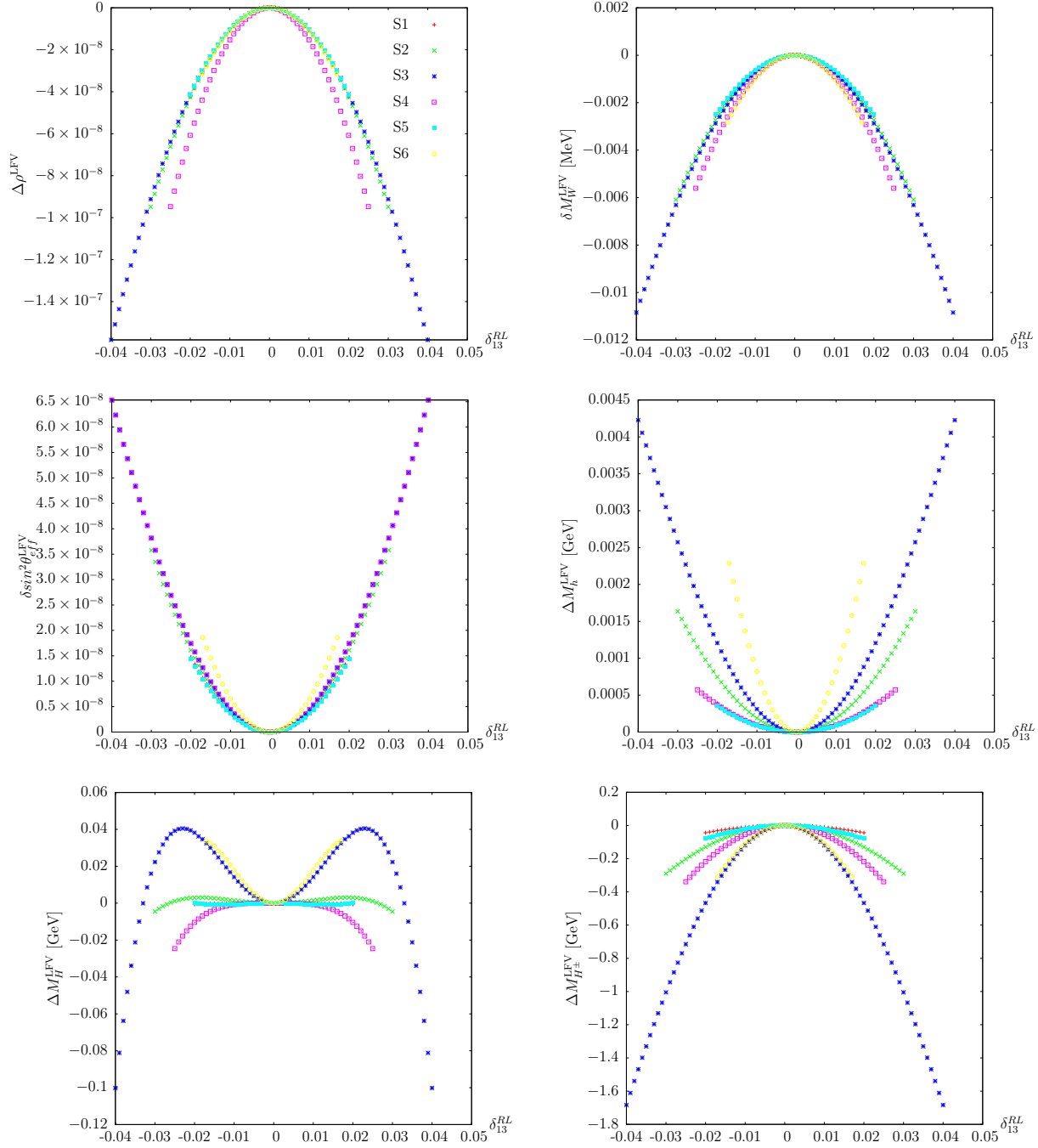


Figure 7: EWPO and Higgs masses as a function of slepton mixing δ_{13}^{RL} for the six points defined in the Tab. 1.

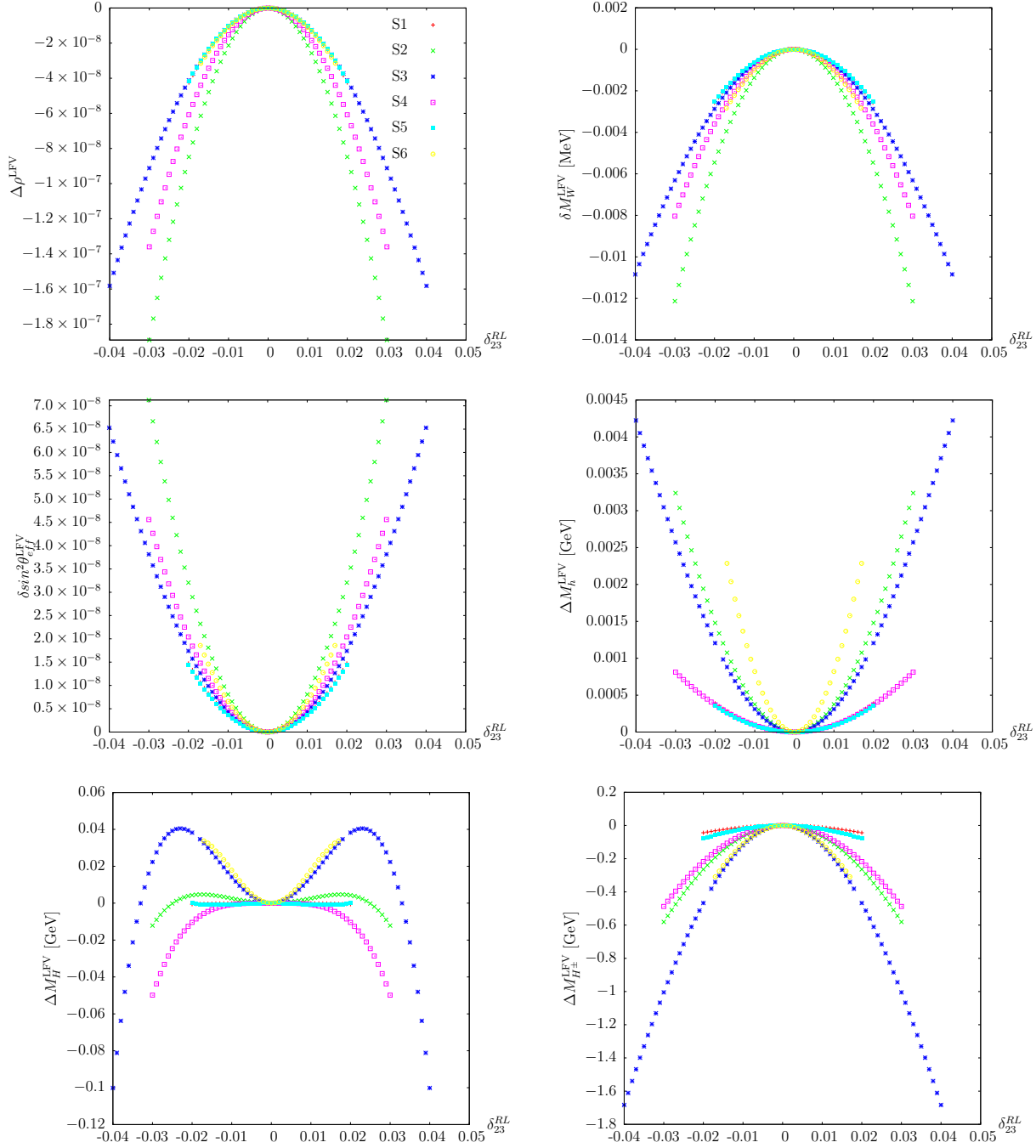


Figure 8: EWPO and Higgs masses as a function of slepton mixing δ_{23}^{RL} for the six points defined in the Tab. 1.

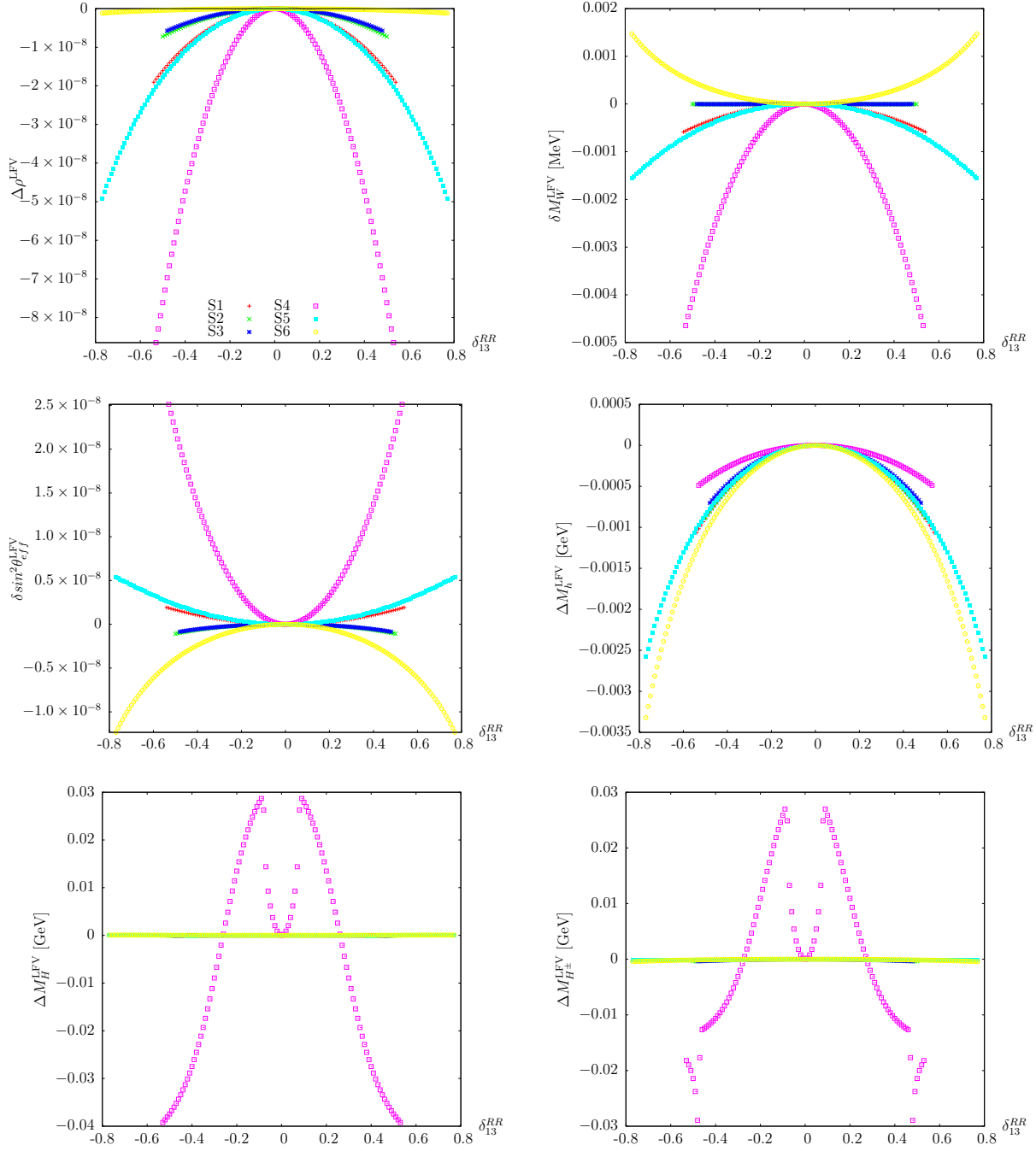


Figure 9: EWPO and Higgs masses as a function of slepton mixing δ_{13}^{RR} for the six points defined in the Tab. 1.

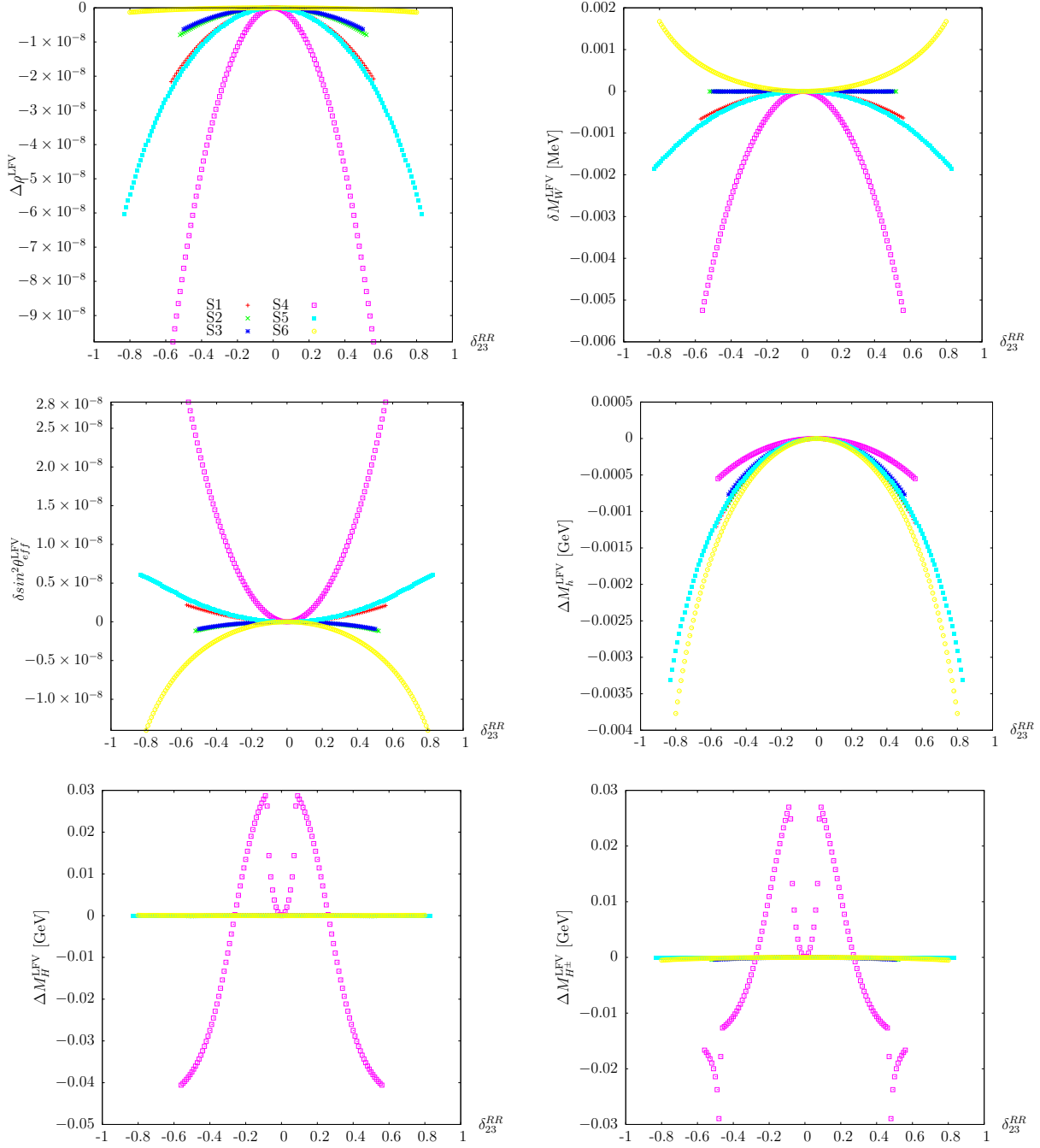


Figure 10: EWPO and Higgs masses as a function of slepton mixing δ_{23}^{RR} for the six points defined in the Tab. 1.

5 Conclusions

We extended Lepton Flavor Violation in the MSSM into the setup of FeynArts and FormCalc; the corresponding model file is part of the latest release of these programs.

The LFV effects are parameterized in a complete set of δ_{ij}^{AB} ($A, B = L, R; i, j = 1, 2, 3$) without any assumption on the physics at the GUT scale. The inclusion of LFV into FeynArts/FormCalc allowed us to calculate the one-loop LFV effects on electroweak precision observables (via the calculation of gauge-boson self-energies) as well on the Higgs-boson masses of the MSSM (via the calculation of the Higgs-boson self-energies). The corresponding results have been included in the code FeynHiggs and are publicly available from version 2.10.2 on.

The numerical analysis was performed on the basis of six benchmark points defined in Ref. [20]. These benchmark points represent different combinations of parameters in the sfermion sector. The restrictions on the various δ_{ij}^{AB} in these six scenarios, provided by experimental limits on LFV processes (such as $\mu \rightarrow e\gamma$) have been taken from Ref. [20], and the effects on EWPO and Higgs-boson masses have been evaluated in the experimentally allowed ranges. In this way we provide a general overview about the possible size of LFV effects and potential new restrictions on the δ_{ij}^{AB} from EWPO and Higgs-boson masses.

The LFV effects in the EWPO turned out to be sizable for δ_{23}^{LL} but (at least in the scenarios under investigation) negligible for the other δ_{ij}^{AB} . The effects of varying δ_{23}^{LL} in the experimentally allowed ranges turned out to exceed the current experimental uncertainties of M_W and $\sin^2\theta_{\text{eff}}$ in the case of heavy sleptons. No new general bounds could be set on δ_{23}^{LL} , however, since the absolute values of M_W and $\sin^2\theta_{\text{eff}}$ strongly depend on the choices in the stop/sbottom sector, which is disconnected from the slepton sector presently under investigation. Such bounds could be set on a point-by-point basis in the LFV MSSM parameter space, however. Looking at the future anticipated accuracies, also lighter sleptons yielded contributions exceeding that precision. It may therefore be possible in the future to set bounds on δ_{23}^{LL} from EWPO that are stronger than from direct LFV processes.

In the Higgs sector, based on evaluations for flavor violation in the squark sector, non-negligible corrections to the light \mathcal{CP} -even Higgs mass as well as to the charged Higgs-boson mass could be expected. The associated theoretical uncertainties exceeded the anticipated future precision for M_h and M_{H^\pm} . Taking the existing limits on the δ_{ij}^{AB} from LFV processes into account, however, the corrections mostly turned out to be small. For the light \mathcal{CP} -even Higgs mass they stay at the few-MeV level. For the charged Higgs mass they can reach $\mathcal{O}(2 \text{ GeV})$, which, depending on the choice of the heavy Higgs-boson mass scale, could be at the level of the future experimental precision. More importantly, the theoretical uncertainty from LFV effects that previously existed for the evaluation of the MSSM Higgs-boson masses, has been reduced below the level of future experimental accuracy.

Acknowledgments

We thank M. Arana-Catania and M.J. Herrero for helpful discussions. The work of S.H. was partially supported by CICYT (grant FPA 2010–22163-C02-01). S.H. and M.R. were supported by the Spanish MICINN’s Consolider-Ingenio 2010 Programme under grant Multi-Dark CSD2009-00064.

References

- [1] Y. Kuno and Y. Okada, *Rev. Mod. Phys.* **73** (2001) 151 [arXiv:hep-ph/9909265].
- [2] H. Nilles, *Phys. Rept.* **110** (1984) 1;
H. Haber and G. Kane, *Phys. Rept.* **117** (1985) 75;
R. Barbieri, *Riv. Nuovo Cim.* **11** (1988) 1.
- [3] L. Hall, V. Kostelecky and S. Raby, *Nucl. Phys.* **B 267**, 415 (1986).
- [4] F. Borzumati and A. Masiero, *Phys. Rev. Lett.* **57** (1986) 961.
- [5] M. Arana-Catania, S. Heinemeyer, M. Herrero and S. Penaranda, *JHEP* **1205** (2012) 015 [arXiv:1109.6232 [hep-ph]]; arXiv:1201.6345 [hep-ph]; arXiv:1405.6960 [hep-ph].
- [6] S. Heinemeyer, W. Hollik and G. Weiglein, *Phys. Rept.* **425** (2006) 265. hep-ph/0412214.
- [7] S. Heinemeyer, W. Hollik, F. Merz, S. Peñaranda, *Eur. Phys. J. C* **37** (2004) 481, hep-ph/0403228.
- [8] ATLAS Collaboration, ATLAS-CONF-2013-014, ATLAS-CONF-2013-025.
- [9] CMS Collaboration, CMS-PAS-HIG-13-005.
- [10] H. Baer et al., arXiv:1306.6352 [hep-ph].
- [11] J. Küblbeck, M. Böhm and A. Denner, *Comput. Phys. Commun.* **60** (1990) 165;
T. Hahn, *Comput. Phys. Commun.* **140** (2001) 418 [arXiv:hep-ph/0012260].
- [12] T. Hahn and C. Schappacher, *Comput. Phys. Commun.* **143** (2002) 54 [arXiv:hep-ph/0105349].
The program and the user's guide are available via www.feynarts.de .
- [13] T. Fritzsche, T. Hahn, S. Heinemeyer, F. von der Pahlen, H. Rzehak and C. Schappacher, to appear in *Comput. Phys. Commun.*, arXiv:1309.1692 [hep-ph].
- [14] T. Hahn and M. Pérez-Victoria, *Comput. Phys. Commun.* **118** (1999) 153 [arXiv:hep-ph/9807565].
- [15] S. Heinemeyer, W. Hollik and G. Weiglein, *Comput. Phys. Commun.* **124** (2000) 76 [arXiv:hep-ph/9812320];
T. Hahn, S. Heinemeyer, W. Hollik, H. Rzehak and G. Weiglein, *Comput. Phys. Commun.* **180** (2009) 1426; see www.feynhiggs.de .
- [16] S. Heinemeyer, W. Hollik and G. Weiglein, *Eur. Phys. J. C* **9** (1999) 343 [arXiv:hep-ph/9812472].
- [17] G. Degrossi, S. Heinemeyer, W. Hollik, P. Slavich and G. Weiglein, *Eur. Phys. J. C* **28** (2003) 133 [arXiv:hep-ph/0212020].

- [18] M. Frank, T. Hahn, S. Heinemeyer, W. Hollik, R. Rzehak and G. Weiglein, *JHEP* **0702** (2007) 047 [arXiv:hep-ph/0611326].
- [19] T. Hahn, S. Heinemeyer, W. Hollik, H. Rzehak and G. Weiglein, to appear in *Phys. Rev. Lett.*, arXiv:1312.4937 [hep-ph].
- [20] M. Arana-Catania, S. Heinemeyer and M. Herrero, *Phys. Rev. D* **88** (2013) 015026 [arXiv:1304.2783 [hep-ph]].
- [21] S. Bilenky, S. Petcov and B. Pontecorvo, *Phys. Lett. B* **67** (1977) 309; W. Marciano and A. Sanda, *Phys. Lett. B* **67** (1977) 303.
- [22] T. Cheng, L.-F. Li, *Phys. Rev. Lett.* **45** (1980) 1908.
- [23] A. Crivellin, L. Hofer and J. Rosiek, *JHEP* **1107** (2011) 017 [arXiv:1103.4272 [hep-ph]].
- [24] S. Heinemeyer, W. Hollik, H. Rzehak and G. Weiglein, *Phys. Lett. B* **652** (2007) 300 [arXiv:0705.0746 [hep-ph]].
- [25] J. Gunion, H. Haber, G. Kane and S. Dawson, *The Higgs Hunter's Guide*, Addison-Wesley, 1990.
- [26] A. Dabelstein, *Nucl. Phys. B* **456** (1995) 25 [arXiv:hep-ph/9503443]; *Z. Phys. C* **67** (1995) 495 [arXiv:hep-ph/9409375].
- [27] A. Brignole, *Phys. Lett. B* **281** (1992) 284; P. Chankowski, S. Pokorski and J. Rosiek, *Phys. Lett. B* **286** (1992) 307.
- [28] S. Gennai et al. *Eur. Phys. J. C* **52** (2007) 383 [arXiv:0704.0619 [hep-ph]].
- [29] The LEP Collaborations, the LEP Electroweak Working Group, the Tevatron Electroweak Working Group, the SLD Electroweak and Heavy Flavour Working Groups, Precision electroweak measurements and constraints on the Standard Model, CERN-PH-EP/2009-023; see <http://www.cern.ch/LEPEWWG> .
- [30] M. Baak et al., [arXiv:1310.6708[hep-ph]].
- [31] M. Veltman, *Nucl. Phys. B* **123** (1977) 89.
- [32] H. Haber and Y. Nir, *Nucl. Phys. B* **335** (1990) 363.
- [33] S. Chatrchyan *et al.* [CMS Collaboration], arXiv:1303.4571 [hep-ex]; Pedrame Bargassa, talk given at “Rencontres de Moriond EW 2014”, <https://indico.in2p3.fr/getFile.py/access?contribId=189&sessionId=0&resId=1&materialId=slides&confId=9116>; Mike Flowerdew, talk given at “Rencontres de Moriond EW 2014”, <https://indico.in2p3.fr/getFile.py/access?contribId=169&sessionId=0&resId=0&materialId=slides&confId=9116>; Paul Thompson, talk given at “Rencontres de Moriond EW 2014”, <https://indico.in2p3.fr/getFile.py/access?contribId=220&sessionId=8>

&resId=0&materialId=slides&confId=9116;
Kevin Einsweiler, talk given at “Rencontres de Moriond EW 2014”,
[https://indico.in2p3.fr/getFile.py/access?contribId=227&sessionId=1
&resId=1&materialId=slides&confId=9116](https://indico.in2p3.fr/getFile.py/access?contribId=227&sessionId=1&resId=1&materialId=slides&confId=9116) .

- [34] P. Bechtle, O. Brein, S. Heinemeyer, G. Weiglein and K. Williams, *Comput. Phys. Commun.* **181** (2010) 138 [arXiv:0811.4169 [hep-ph]]; *Comput. Phys. Commun.* **182** (2011) 2605 [arXiv:1102.1898 [hep-ph]];
P. Bechtle, O. Brein, S. Heinemeyer, O. Stål, T. Stefaniak, G. Weiglein and K. Williams, *Eur. Phys. J. C* **74** (2014) 2693 [arXiv:1311.0055 [hep-ph]].
- [35] M. Awramik, M. Czakon, A. Freitas and G. Weiglein, *Phys. Rev. D* **69** (2004) 053006 [arXiv:hep-ph/0311148].
- [36] M. Awramik, M. Czakon, A. Freitas and G. Weiglein, *Phys. Rev. Lett.* **93** (2004) 201805 [arXiv:hep-ph/0407317].
- [37] T. Hahn, W. Hollik, J.I. Illana, S. Peñaranda, arXiv:hep-ph/0512315.